Available online at www.sciencedirect.com

SciVerse ScienceDirect

Nuclear Physics A 875 (2012) 139–159

NUCLEAR PHYSICS A

www.elsevier.com/locate/nuclphysa

Towards an understanding of staggering effects in dissipative binary collisions

M. D'Agostino [a,b,*], M. Bruno [a,b], F. Gulminelli [c], L. Morelli [a,b], G. Baiocco [a,b,c], L. Bardelli [d,e], S. Barlini [d], F. Cannata [b], G. Casini [d], E. Geraci [f,e], F. Gramegna [g], V.L. Kravchuk [g], T. Marchi [g,h], A. Moroni [i], A. Ordine [j], Ad.R. Raduta [k]

[a] *Dipartimento di Fisica dell'Università, Bologna, Italy*
[b] *INFN, Bologna, Italy*
[c] *CNRS, UMR6534, LPC, F-14050 Caen cédex and ENSICAEN, UMR6534, LPC, F-14050 Caen cédex, France*
[d] *INFN, Firenze, Italy*
[e] *INFN, Catania, Italy*
[f] *Dipartimento di Fisica dell'Università, Catania, Italy*
[g] *INFN, Laboratori Nazionali di Legnaro, Italy*
[h] *Dipartimento di Fisica dell'Università, Padova,Italy*
[i] *INFN, Milano, Italy*
[j] *INFN, Napoli, Italy*
[k] *NIPNE, Bucharest-Magurele, POB-MG6, Romania*

Received 19 June 2011; received in revised form 20 September 2011; accepted 25 November 2011

Available online 9 December 2011

Abstract

The reactions $^{32}S + ^{58,64}Ni$ are studied at 14.5 A MeV. Evidence is found for important odd–even effects in isotopic observables of selected peripheral collisions corresponding to the decay of a projectile-like source. The influence of secondary decays on the staggering is studied with a correlation function technique. It is shown that this method is a powerful tool to get experimental information on the evaporation chain, in order to constrain model calculations. Specifically, we show that odd–even effects are due to interplay between pairing effects in the nuclear masses and in the level densities.

* Corresponding author at: INFN, Bologna, Italy.
E-mail address: dagostino@bo.infn.it (M. D'Agostino).

0375-9474/$ – see front matter
doi:10.1016/j.nuclphysa.2011.11.011

Keywords: NUCLEAR REACTIONS ^{58,64}Ni(^{32}S, X), $E = 14.5$ MeV/nucleon; measured fragment yield and charge distribution; deduced reaction mechanism features, odd–even effects, secondary evaporation, relative kinetic energy correlation functions. Comparison with GEMINI evaporation model. GARFIELD detector array and ring counter

1. Introduction

Experimental studies of odd–even effects in fragment production have been performed since a long time. Nevertheless the analysis of these results has not produced clear-cut conclusions about their interpretation [1–5]. A priori, these effects point to the pairing residual interaction and its dependence on temperature. Getting experimental information on this issue is of importance both in nuclear physics [6] and in nuclear astrophysics [7,8]. Understanding the origin of odd–even effects is also relevant for studies on symmetry energy [9], which can be linked to the isotopic distributions [10] if these latter are not too much perturbed by secondary decays [11–13].

In theoretical studies no staggering is associated to the finite temperature yields, but odd–even effects appear in the asymptotic yields after evaporation [14,15]. This observation suggests that odd–even effects are low temperature effects associated to the evaporation phase. Two physical ingredients which can in principle be associated to odd–even effects exist in evaporation models, namely level densities and binding energies. Then the question arises whether the observed staggering in the production yields is just a straightforward consequence of the pairing effect in nuclear masses.

This problem was recently raised in Ref. [2], where odd–even effects in the reaction $p + \mathrm{Fe}$ at 1 A GeV at the FRS were studied. The idea proposed in that paper is that indeed nuclear masses determine the observed staggering through the last step of the evaporation chain[1]: the hypothesis is that, independent of the initial thermodynamic condition of the excited pre-fragments, the very last evaporation step concerns either a neutron or a proton, depending on the relative separation energies of the two particles. The staggering in the yields would then reflect the staggering in the neutron–proton separation energies due to the pairing and Wigner term in the mass formula. This idea predicts correctly the trend of the observed staggering in the experiment at the FRS. However it does not reproduce the amplitude of the staggering quantitatively: the experimental oscillations are less important than the ones predicted in this simple scenario. This suggests that the previous evaporation steps may also play a role.

In a recent paper [16], we have reported on an experimental study of staggering in S + Ni collisions at 14.5 A MeV. To explore in detail the possible relationship of odd–even effects to the isospin of the emitting sources, we have measured the yields of isotopes for reaction pairs differing only in the values of the isospin. We have shown that important odd–even effects exist in carefully selected peripheral events, while they are masked in central collision by the strongly decreasing behavior of the production yield as a function of the fragment size. A detailed study of the most probable decays that can contribute to the yield of the different isotopic chains has additionally indicated that the lowest emission threshold for particle production cannot be the unique factor governing the staggering, and a quantitative control on the population at the last-but-one evaporation step is important to assess the physical origin of the staggering.

[1] Throughout the paper, we will implicitly define the last step of the evaporation chain as the last particle emission. This decay does not necessarily lead to the ground state of the daughter nucleus, but the subsequent gamma emission chain does not modify the isotopic yields and does not need to be considered for the purpose of this paper.

To make progress on this issue, in the present paper we estimate directly from experimental data the effect of secondary evaporation on the staggering using a correlation function based technique. No specific model is assumed for the source characteristics and decay probabilities. We show that odd–even effects are already present in fragment yields excited above the particle emission threshold, in qualitative agreement with GEMINI calculations.

This indicates that in order to quantitatively understand the observed staggering, both pairing effects on the nuclear masses and on the level densities should be considered.

2. Experimental distributions

The measurements were performed at the TANDEM–ALPI acceleration system of the Legnaro National Laboratory. The detecting device is composed by the GARFIELD detector [17] covering almost completely the angular range of polar angle from 30° to 85° and an annular three-stage detector (Ring Counter) [18] covering laboratory forward angles from 5.3° to 17.5°. The detecting device can identify from light charged particles to heavy fragments with an energy threshold of the order of few hundreds of A keV.

The results here presented come from the comparison of the data for the two reactions $^{32}\mathrm{S} + {}^{58}\mathrm{Ni}$ and $^{32}\mathrm{S} + {}^{64}\mathrm{Ni}$ at 14.5 A MeV. As explained in detail in Ref. [16], the sorting of the measured events as a function of the centrality has been performed with the method of the "shape analysis" [19], as in other intermediate and high energy experiments performed with $\simeq 4\pi$ detectors [20,21]. Events characterized by the detection of at least 50% of the total incoming parallel momentum were studied as a function of the total detected charge. Due to the energy thresholds, the quasi-target products are not detected, so that "peripheral" events can be selected by the additional conditions $Z_{tot} \leqslant 25$ and $\theta_{flow} \leqslant 40°$. A comparison to the GEMINI [22] evaporation code suggests that for both reactions these events are associated to the evaporation from a quasi-projectile source with $\langle E^* \rangle \approx 1$ A MeV, $\langle Z \rangle \approx 16$, $\langle A \rangle \approx 32$, and a triangular distribution of angular momentum between $J_{\min} = 0\hbar$ and $J_{\max} = 16\hbar$. More details on the experiment and data selection can be found in Ref. [16].

Odd–even effects in the decay of this source are clearly established even in relatively inclusive observables. This is shown in Fig. 1 [16], which displays the elemental fragment ($Z \geqslant 3$) distribution for the two reactions.

The charge (mass) distributions presented in this paper, unless explicitly stated, have been normalized to the number of events and therefore they represent the elemental multiplicity of a given charge (mass).

To highlight the odd–even effects, the bottom panel of Fig. 1 displays the ratio between the elemental charge distribution and a smoothed distribution obtained by a parabolic interpolation of the measured yields over 5 consecutive points.

Considering that for almost all the isotopically resolved yields (that is up to $Z = 8$) the most abundant isotope of each element is $N = Z$, as shown in Fig. 7 of Ref. [16], the staggering observed in the global distributions Fig. 1 can be interpreted as dominance of even–even isotopes over odd–odd ones as one would naively expect from the pairing contribution in the isotope masses.

The striking persistence of pairing effects in the fragmentation phenomenon which is thought to occur at finite temperature, has been tentatively interpreted in Ref. [2] as an effect of the last step of the evaporation chain. This decay is almost deterministically established by the Q-value of the decay to the daughter nucleus energy states which lie below the threshold for particle

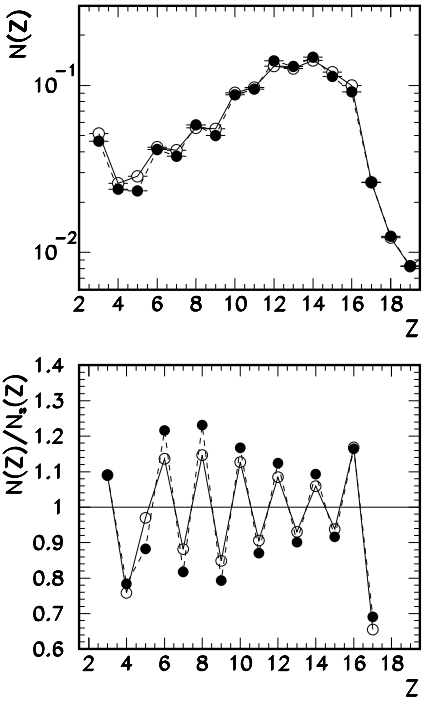

Fig. 1. (Color online.) Elemental fragment ($Z \geqslant 3$) distribution from the decay of the quasi-projectile source formed in $^{32}S + ^{58}Ni$ (full symbols, dashed line) and $^{32}S + ^{64}Ni$ (open symbols, full line). Upper part: Fragment distribution normalized to the total number of peripheral events. Bottom part: Ratio of the fragment distribution by a smoothed distributions obtained by a parabolic interpolation over 5 consecutive points. Lines are drawn to guide the eye.

emission. This latter is maximal if the daughter nucleus presents an extra binding due to pairing, since the pairing shift increases the particle emission threshold.

This simple explanation however only holds if the last evaporation step changes the isotopic content $N - Z$ of the decaying nucleus. This is indeed the case if the last evaporation step concerns only neutron and proton evaporation, but not if the last emitted particle is an α particle. It comes out that the nucleon decay channel is dominant for $N = Z + 1$ isotopes, but the same is not true for $N = Z$. This is demonstrated in Fig. 2, which compares the energy of the first particle-unstable level [23,24] of a given daughter nucleus, to the particle emission thresholds of this latter, as obtained from mass differences. In this figure, in order to disentangle the staggering behavior from the rapidly decreasing trend of the mass distribution, the measured yield of each isotope is normalized to the total detected yield for the considered element.

We can see that in the case of the $N = Z + 1$ isotopic chain the first particle unstable state approximately coincides with the Q-value for neutron emission, which presents a staggering behavior due to the pairing term in the nuclear mass. This trend is nicely followed by the experimental yields for both reactions, as shown in Fig. 2 [16]. In the case of the $N = Z$ isotopic chain, which is responsible of the global staggering behavior of the elemental distribution, the situation is less clear. Indeed the lowest emission threshold for $N = Z$ light nuclei typically corresponds to α decay, with the only exception of ^{14}N. The α decay preserves the isospin difference $N - Z$ and thus shows a smooth behavior, which does not correspond to the staggering trend of the yields. This in turn means that the extra yield of even–even isotopes cannot be simply due to the energy

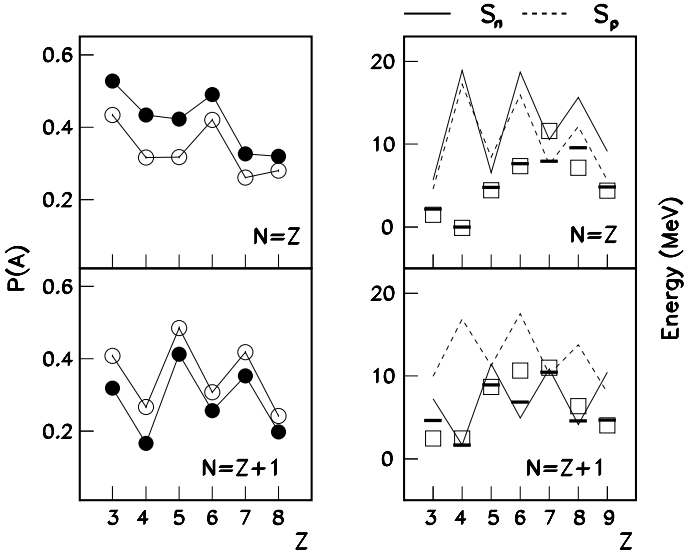

Fig. 2. (Color online.) Fragment ($3 \leqslant Z \leqslant 8$) isotopic distribution normalized to the total elemental yield for $^{32}S + ^{58}Ni$ (full symbols) and $^{32}S + ^{64}Ni$ (open symbols) corresponding to the isotopic chain $N = Z$ (upper part) and $N = Z + 1$ (lower part). For each isotopic chain, the panels on the right show the energy of the lowest unstable state (thick lines) decaying in a given daughter isotope, the Q-value for alpha decay (open squares) and the neutron (S_n) and proton (S_p) separation energies.

balance of the last evaporation step, but has to be related to the isotopic population of the excited nuclei prior to their last decay by particle emission.

This expectation is confirmed by the GEMINI model, which is able to describe satisfactorily the main features of this same data set [16] and to very well reproduce the even–odd staggering observed in fragmentation data, when applied to simulate the decays of the prefragments generated by a dynamical model [15]. As in Ref. [16], an excited source with Gaussian distributed parameters centered in $\langle E^* \rangle = 1$ A MeV, $\langle Z \rangle = 16$, $\langle A \rangle = 32$ and a triangular distribution of angular momentum between $J_{\min} = 0\hbar$ and $J_{\max} = 16\hbar$ is considered. The "warm" elemental yield, obtained by summing up the cold products emitted in the last step by the same parent, is represented in Fig. 3. We can see that this distribution is not smooth. To better evidence the staggering already present in the excited yields, the bottom part of the figure shows the same yield divided by a parabolic interpolation over 5 consecutive points as in Fig. 1 above.

From this discussion it is clear that, in order to fully understand the staggering in final measured yields, it is necessary to have experimental information on the population of parent nuclei at the previous step of the decay chain. To this aim, we present in the next section a correlation function study of isotopically resolved pairs. This technique allows us, at least in some selected cases, to reconstruct the primary yields of decaying nuclei.

3. Correlation functions

To address the problem of understanding quantitatively odd–even effects and in the long run gather information on pairing and isovector properties of the nuclear level density, we propose in this section a back-tracing technique based on correlation functions of the relative kinetic energy of isotope pairs.

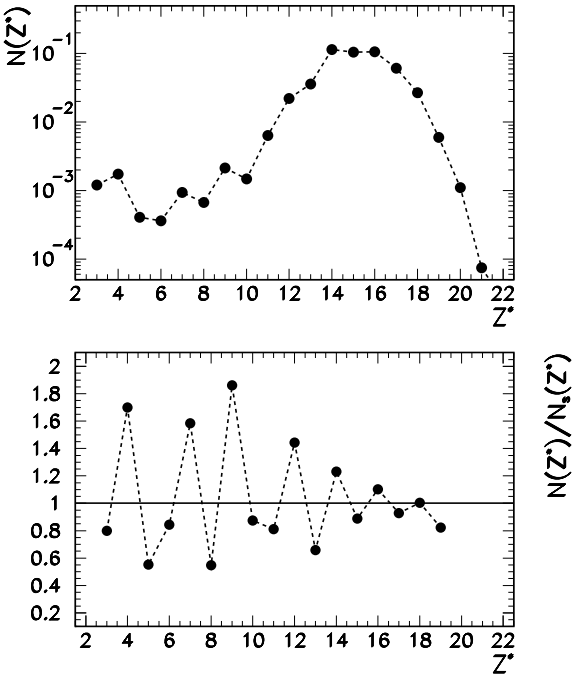

Fig. 3. (Color online.) Elemental "warm" fragment ($Z \geqslant 3$) distribution from the decay of an excited source with $\langle A \rangle = 32$, $\langle Z \rangle = 16$, $\langle E^* \rangle = 1$ A MeV and a triangular distribution of angular momentum between $J = 0\hbar$ and $J = 16\hbar$, within the GEMINI evaporation model. Upper part: inclusive charge distribution. Lower part: Ratio of the fragment ($Z \geqslant 3$) distribution shown in the upper part by smoothed distributions obtained by a parabolic interpolation over 5 consecutive points.

If we concentrate on light nuclei ($3 \leqslant Z \leqslant 8$), their discrete spectrum is so extended that the last particle evaporation step takes place typically from a discrete resonance, which can at least in principle be recognized as a peak in a relative kinetic energy two-body correlation function.

To fully reconstruct the last-but-one evaporation step one should measure also neutron-charged products correlations functions which is not possible with our detector. Another limitation is given by the statistics of the experiment. Because of that, we analyze peripheral events as a whole, which corresponds to a distribution of sources in A and E^*. Due to these problems, we will not be able to extract any quantitative information on the temperature dependence of the pairing. However, we can experimentally assess how much the fragment yield is influenced by the last particle decay step, when this latter consists of a charged particle decay. This will give us important information on how relevant is this last step in the production of the odd–even effect.

3.1. The correlation function technique

Correlation functions, initially introduced to measure distant astronomical objects [25], have shown their predictive power over the years independent of the specific reaction and decay mechanism. In particular they have been intensively used as a tool to investigate source sizes and freeze-out conditions for nucleus–nucleus collisions at intermediate [26] and relativistic [27] incident energies.

This same methodology is at the basis of very powerful model-independent imaging techniques [28] and is routinely used to determine the spectroscopic characteristics of dripline nuclei produced in direct reactions [29]. This flexibility of the correlation function tool makes it a very sound and powerful technique to experimentally access loosely bound and unbound states.

Experimentally the two-particle correlation function may be defined as:

$$\sum_{(\vec{p}_1-\vec{p}_2)^2/2\mu=E_{rel}} Y_{12}(\vec{p}_1,\vec{p}_2) = C\big[1+R(E_{rel})\big] \sum_{(\vec{p}_1-\vec{p}_2)^2/2\mu=E_{rel}} Y_1(\vec{p}_1)Y_2(\vec{p}_2), \tag{1}$$

where Y_{12} is the two-particle coincidence yield of a given pair of particles with their individual momenta $\vec{p}_1$ and $\vec{p}_2$, respectively, and the $Y_i(\vec{p}_i)$ are the single particle yields for the two particles measured under the same impact parameter selection but not in the same event. The summations on both sides of the equation run over pairs of momenta $\vec{p}_1$ and $\vec{p}_2$ corresponding to the same bin in relative energy E_{rel}. The correlation function describes how the correlation between interacting particles measured in the same event differs from the underlying two-particle phase space. This phase space can be modeled by mixing the single particle distributions of particles from different events [30]. The correlation constant C is chosen [31] as the ratio between the total (integrated over momentum) number of generated mixed events and the total number of coincident yields: $C = \sum Y_{12}/\sum(Y_1 Y_2)$.

To investigate the decay of particle unbound states it is necessary to consider the modifications of the two particle phase space by the long range Coulomb and short range nuclear interactions and to disentangle these contributions. We have chosen to parametrize the Coulomb contribution by an empirical expression [32,33]

$$1 + R_{Coul}(E_{rel}) = 1 - \exp\big[-(E_{rel}/E_c)^{\gamma}\big] \tag{2}$$

which vanishes at zero relative energy and reaches unity at large relative energy. This parametrization was recently shown [34] to be flexible enough to well reproduce the background of fragmentation reactions in the Fermi energy domain.

Given this relationship, we obtain a practical expression for the correlation function as a function of relative energy E_{rel}

$$1 + R(E_{rel}) = 1 + R_{Coul}(E_{rel}) + R_{nuc}(E_{rel}), \tag{3}$$

where

$$R_{nuc}(E_{rel}) = \frac{1}{(2S_1+1)(2S_2+1)} \frac{h^3}{4\pi V_f \mu\sqrt{2\mu E_{rel}}} e^{-E_{rel}/T_{eff}} \times \frac{1}{\pi}\sum_i (2J_i+1)\frac{\Gamma_i/2}{(E_{rel}-E_i^*)^2+\Gamma_i^2/4}(\text{B.R.}). \tag{4}$$

Here S_1 and S_2 are the spins of the considered particles, μ is their reduced mass, V_f is the effective emitting source volume, T_{eff} is the associated effective temperature, J_i, E_i^*, Γ_i are the spin, excitation energy and width of the level i, and (B.R.) is the branching ratio for decay to the measured channel. It is worth mentioning that this parametrization has been successfully used in fragmentation reactions not only to reproduce measured correlations, but even to deduce spin and parity of excited states unknown to traditional spectroscopic studies [34].

Only levels where spins, excitation energies, widths of the levels and branching ratios were experimentally measured [23,24] were considered. Some modifications in the widths were allowed to account for the finite efficiency of the detection apparatus, as it will be discussed in detail in

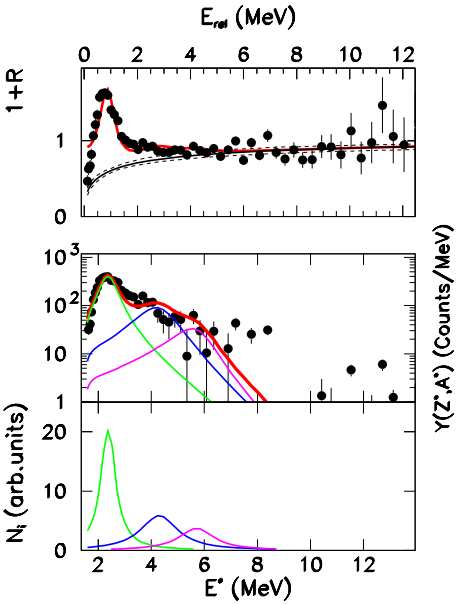

Fig. 4. (Color online.) Upper part: d–α relative kinetic energy correlation function (symbols) measured in peripheral $^{32}S + {}^{58}Ni$ collisions and fitted through Eq. (4) (thick solid line). The obtained Coulomb background (thin solid line) is also indicated together with its uncertainties (dashed lines). Middle part: experimental population of primary ^{6}Li parent (symbols) and single excited state contributions (thin lines) together with their sum (thick line) as a function of the excitation energy: $E^* = E_{rel} + Q_V$, with $Q_V = Q$-value of the decay. Lower part: extracted N_i Breit–Wigner contributions of the different populated excited states.

the next section. The Coulomb background parameters E_c, γ are free parameters of the fit. The same is true for the parameters V_f, T_{eff}, which would represent a physical source volume and temperature only in the idealized situation of a single decay step of a fully equilibrated source in the absence of any collective flow and experimental deformation. Qualitatively, collective energy components act in the direction of increasing V_f in respect to a physical volume, which leads to a suppression of high-lying resonances, while efficiency issues point to an increase of T_{eff} in respect to a physical temperature, with an opposite effect on the resonant population. Because of this correlation, the parameter space is degenerate and no physical meaning can be attributed to the V_f, T_{eff} values extracted from Eq. (4).

3.2. Extraction of primary fragments

Examples of typical correlation functions and resulting fits via Eq. (4) are shown in the top panels of Figs. 4 and 5. The errors associated to the fit parameters E_c, γ produce an upper and lower bound for the estimated Coulomb background, which are indicated by the dashed lines.

Primary yields are calculated by multiplying the nuclear contribution $R - R_{Coul}$ of the correlation function for the uncorrelated yield of Eq. (1), $Y_{cor}(E^*) = (R(E^*) - R_{Coul}(E^*)) \sum_E Y_1 Y_2$ [32,33]. This experimentally reconstructed primary population is shown by full symbols for some selected nuclei in the middle panel of Fig. 4 and bottom panels of Figs. 5, together with the contributions from the different parent excited levels entering in Eq. (4), shown as lines. The bottom panel of Fig. 4 additionally shows the extracted Breit–Wigner distribution of the different popu-

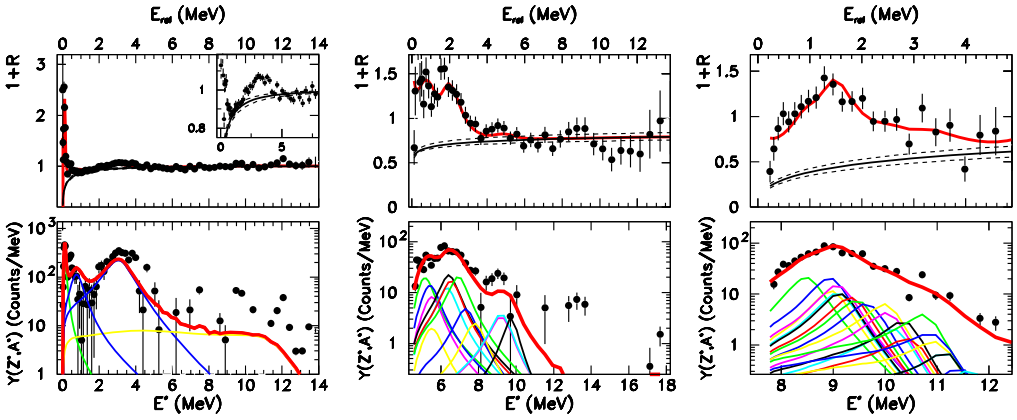

Fig. 5. (Color online.) Upper part: representative relative kinetic energy correlation functions (symbols) of different isotopes measured in peripheral $^{32}S + ^{58}Ni$ collisions and fitted through Eq. (4) (thick solid line). The obtained Coulomb background (thin solid line) is also indicated together with its uncertainties (dashed lines). Lower part: experimental population of primary parents (symbols) and single excited state contributions (thin lines) together with their sum (thick line) as a function of the excitation energy: $E^* = E_{rel} + Q_V$, with $Q_V = Q$-value of the decay. From left to right: α–α correlations and corresponding excited states of ^{8}Be (a view of the correlation function around 3 MeV is shown in the insert), α–^{6}Li correlations and corresponding excited states of ^{10}B, p–^{13}C correlations and corresponding excited states of ^{14}N.

lated excited states. We can notice that the peaks of the correlation function closely correspond to the resonant energies. It is also interesting to remark that the different excited states significantly contribute to a large interval of relative energy which extends relatively far from the resonance peak in a non-symmetric way. The lack of symmetry is due to the combined effect of the phase space factor $1/\sqrt{(E_{rel} 2\mu_{12})}$ which deforms the Breit–Wigner distributions, the suppression factor $\exp(-E_{rel}/T_{eff})$ which accounts for temperature and the distribution of the uncorrelated yield $Y_1 Y_2$ of Eq. (1), Maxwellian-like shaped, as well as non-equilibrium effects that can be present in the sample. Further distortions come from efficiency effects and will be discussed in the next chapter. The errors of the reconstructed yields are calculated by taking into account the statistics of correlated and uncorrelated pairs in each bin of relative energy and the propagation of the errors on E_c and γ in the Coulomb background subtraction.

The systematic error in the reconstructed yield can be estimated by the difference between this correlated yield $Y_{cor}(E^*)$ and the expected resonant yield from Eq. (4), $Y_{res}(E^*) = R_{nuc}(E^*) \sum_E Y_1 Y_2$. This latter quantity is shown by thick lines in Figs. 4, 5.

The main uncertainty is associated to the highest relative energies, due to the lack of statistics of the data, the possible inadequacy of Eq. (2) to correctly account for all the different sources of background and to the incomplete spectroscopic information of the tables of Refs. [23,24].

The global capability of Eqs. (2), (3), (4) to extract the yields of excited parents was checked for the ideal case of only one level plus the Coulomb interaction, with a simulation performed with the SMM model [36], by letting decay a ^{6}Li in its first excited state. The reconstructed primary yield corresponds to 99.6% of the SMM generated and filtered resonant ^{6}Li population.

The total primary population of a given isotope at the last-but-one evaporation step $Y(A^*, Z^*)$ is calculated by integrating over the excitation energy the primary yields given in the bottom part of Figs. 4 and 5. The primary yields obtained by this procedure for the unstable ^{8}Be have been already reported in Fig. 2.

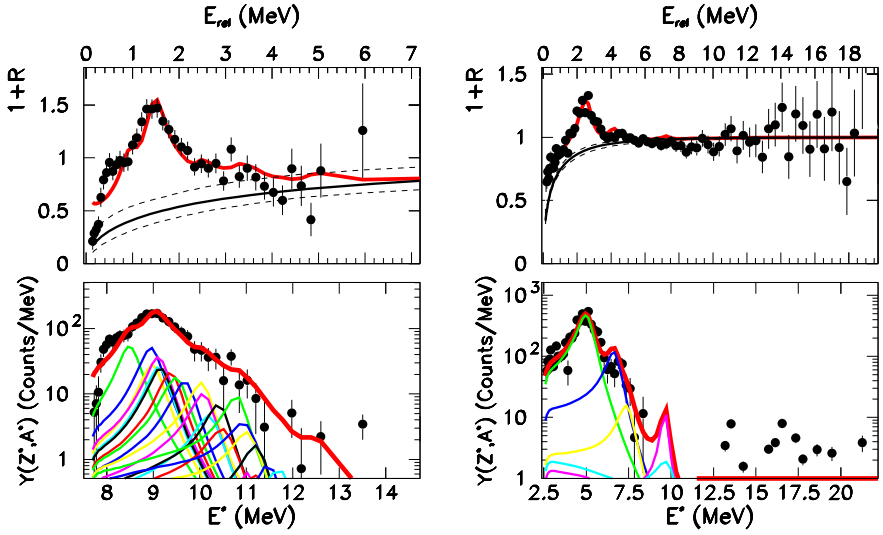

Fig. 6. (Color online.) Upper part: relative kinetic energy correlation functions (symbols) of different isotopes measured in the whole sample of $^{32}S + ^{58}Ni$ collisions and fitted through Eq. (4) (line). The obtained Coulomb background is also indicated together with its uncertainty (dashed lines). Lower part: experimental population of primary parents (symbols) and single excited state contributions (thin lines) together with their sum (thick line) as a function of the excitation energy: $E^* = E_{rel} + Q_V$, with $Q_V = Q$-value of the decay. From left to right: p–^{13}C correlations and corresponding excited states of ^{14}N, t–α correlations and corresponding excited states of ^{7}Li.

Interestingly enough, some excited levels which energetically lie above the lowest threshold for particle emission in the daughter nucleus contribute to the data. To give an example, most of the correlated yield associated to the $\alpha + ^{6}Li$ correlation function presented in Fig. 5 is associated to excited levels of ^{10}B around $E^* = 6.6$ MeV, lying about 300 keV above the threshold for the ^{6}Li decay in $\alpha + d$ and below the separation energy for the neutron emission for this daughter nucleus. Since the $\alpha + d$ correlation function (shown in Fig. 4) was measured, it should be interesting for this case to perform a 3-body decay correlation $\alpha + \alpha + d$ to calculate the amount of primary ^{10}B fragments before their last step of the decay.

Unfortunately, due to the limited statistics associated to the peripheral sample, we can neither perform 3-body correlations nor show other cases of successive decays. To show however that the $\alpha + ^{6}Li$ is not a single case of possible ternary decays, we analyzed the whole sample, obtained for the detected events without any selection on the collision mechanism. In Fig. 6 we show the correlation function $p + ^{13}C$, already shown in Fig. 5 for peripheral events.

The fact that high-lying resonances appear more clearly in the inclusive sample shows that a higher statistics would allow to explore a higher range of excitation energies of the parent nuclei, and have a better reconstruction of the evaporation chain. We also show in Fig. 7 the $p + ^{7}Li$ correlation function, corresponding to the decay of $^{8}Be^*$. The excitation energy of the parent $^{8}Be^*$ overcomes of about 2 MeV, with non negligible yield, the threshold for $\alpha + t$ emission of $^{7}Li^*$, which is below the separation energy for neutron emission. Also the correlation function for $t + \alpha$ is measurable, as shown in Fig. 6.

These examples show that the emission is not necessarily associated to the lowest particle emission threshold, but it depends in a more complicated way on the history of the evaporation chain.

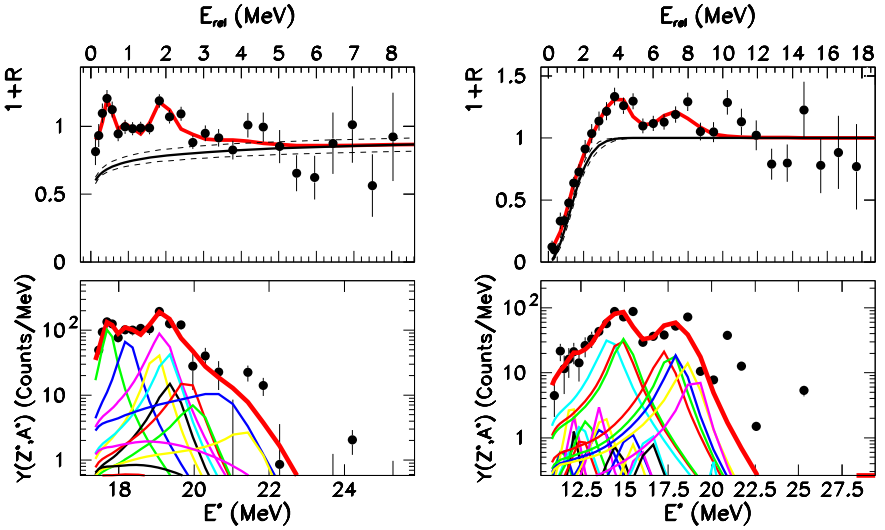

Fig. 7. (Color online.) Upper part: relative kinetic energy correlation functions (symbols) of different isotopes measured in the whole sample of $^{32}S + ^{58}Ni$ collisions and fitted through Eq. (4) (line). The obtained Coulomb background is also indicated together with its uncertainty (dashed lines). Lower part: experimental population of primary parents (symbols) and single excited state contributions (thin lines) together with their sum (thick line) as a function of the excitation energy: $E^* = E_{rel} + Q_V$, with $Q_V = Q$-value of the decay. From left to right: p–^{7}Li correlation and corresponding excited states of ^{8}Be, α–^{9}Be correlation and corresponding excited states of ^{13}C.

The population of different primary nuclei reconstructed via Eq. (4) and their average excitation energy are shown in Fig. 8. The possible contribution from higher mass compounds due to the evaporation of $Z \geqslant 3$ fragments could not be evaluated because of the lack of statistics. However, GEMINI calculations already used to describe this same data set in Ref. [16] predict that the probability of evaporating fragments in the last evaporation step is small, of the order of 7%.

The decay channels contributing to the excited yields are given in Table 1. This table shows that at least three channels are measured for each element, and most populated particle unstable levels significantly contribute to the measured yield. This guarantees that no trivial autocorrelations between the Z of the daughter and the Z of the parent is at the origin of the behavior of the "warm" yields. The huge number of contributing levels also suggests that a complete realistic description of the discrete part of the light fragments level density, with the correct statistical weight of the different levels, will be necessary to have quantitative statistical model predictions of the observed isotopic yields.

The yields of "warm" fragments of charge Z^* have been normalized as:

$$P(Z^*) = \frac{\sum_{A^*} Y(A^*, Z^*)}{\sum_{A^*} Y_{12}(A^*, Z^*)} \tag{5}$$

where two different estimations of the yield $Y(A^*, Z^*)$ of a primary fragment (A^*, Z^*) are extracted from correlation functions ($Y_{cor}(A^*, Z^*)$) and from Eq. (4) ($Y_{res}(A^*, Z^*)$), respectively. The denominator of Eq. (5) is given by the sum of the coincidence yields of Eq. (1) over all the isotope pairs with sum of charges equal to Z^*. In this way $P(Z^*)$ represents the fraction of the coincidence yield corresponding to the emission by "warm" pre-fragments.

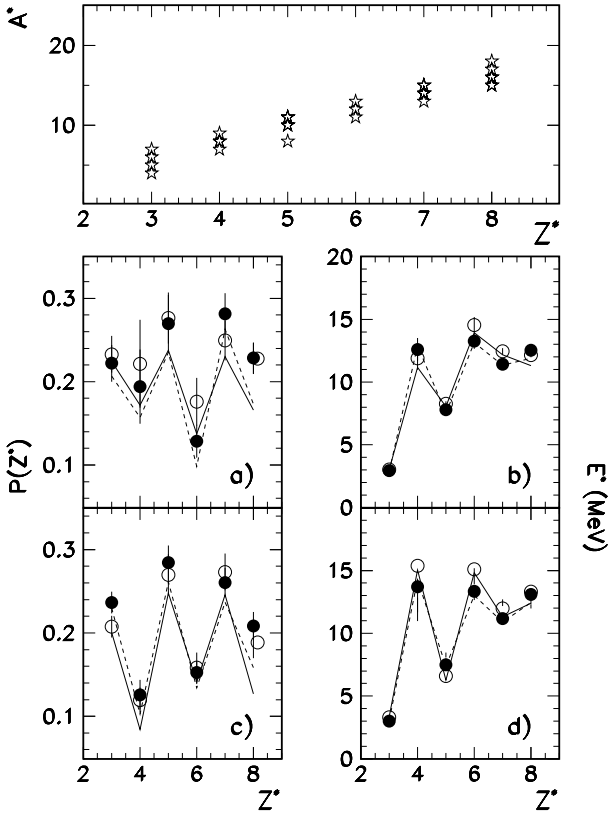

Fig. 8. (Color online.) Upper part: isotopes reconstructed (in at least one of their lowest lying particle unstable excited states) by the correlation function technique in the two data sets. Lower part: extracted population of the different primary fragments (left) and their average excitation energy (right) for the $^{32}S + {}^{58}Ni$ (full symbols and dashed lines) and $^{32}S + {}^{64}Ni$ (circles and full lines) data set. Panels a, b: peripheral sample. Panels c, d: all well detected events.

It is evident that the reconstructed "warm" yields keep on showing the staggering, and the fact of restricting the analysis to the peripheral sample (panels a, b in Fig. 8) does not modify the observed trend. This result means that the reaction dynamics or the previous evaporation chain, essentially coming from continuum states, play a role in establishing odd–even effects, and these latter are not a simple effect of the energetic balance of the last evaporation step.

Particularly striking is the fact that this staggering shows an opposite trend in respect to the experimental asymptotic distributions shown in Fig. 1. This fact can be qualitatively understood as a level density effect: even–even nuclei have a lower density of levels at low energy because of the pairing gap, which leads to a reduced population at the last-but-one evaporation step.

4. Systematic errors and corrections

In Fig. 8 the filled ($^{32}S + {}^{58}Ni$) and empty ($^{32}S + {}^{64}Ni$) circles are associated to the numerical integration of the estimated correlated yield Y_{cor}, once the Coulomb background is subtracted. The error bars give statistical errors as well as the error propagation of the fit parameters. Conversely the lines correspond to the integral of the fitting function Eq. (4) Y_{res} containing all

Table 1
Charge of the "warm" parent nuclei, measured decay channels contributing to the excited yields, maximal observed excitation energy, number of unstable levels implemented in the correlation function analysis [23,24], excitation energy and relative contribution of the dominant states.

Z^*	Decay channel	$E^*_{\max}$ (MeV)	N_{levels}	Most probable levels: E^* (MeV), %
3	$d + {}^3\mathrm{He}$	20.	3	
	$d + \alpha$	8.	3	2.186 (66%), 4.31 (22%)
	$t + \alpha$	9.	3	
4	$p + {}^6\mathrm{Li}$	9.	3	
	$p + {}^7\mathrm{Li}$	20.	10	
	$p + {}^8\mathrm{Li}$	20.	3	
	$\alpha + \alpha$	12.	2	3.03 (82%), 11.35 (12%)
5	$p + {}^7\mathrm{Be}$	3.	2	
	$p + {}^9\mathrm{Be}$	11.	6	
	$\alpha + {}^6\mathrm{Li}$	10.	13	4.774 (12%), 6.025 (11%), 6.56 (10%)
	$\alpha + {}^7\mathrm{Li}$	17.	13	
6	$p + {}^{11}\mathrm{B}$	19.	9	16.57 (10%)
	$\alpha + {}^7\mathrm{Be}$	15.	6	10.68 (8%)
	$\alpha + {}^9\mathrm{Be}$	17.	17	11.95 (6%), 12.10 (8%), 12.44 (6%)
7	$p + {}^{12}\mathrm{C}$	5.	3	2.36 (5%), 3.50 (6%)
	$d + {}^{12}\mathrm{C}$	15.	14	
	$p + {}^{13}\mathrm{C}$	12.	17	8.49 (5%), 8.96 (4%)
	$\alpha + {}^{10}\mathrm{B}$	23.	28	
	$\alpha + {}^{11}\mathrm{B}$	22.	23	
8	$p + {}^{14}\mathrm{N}$	12.	4	
	$\alpha + {}^{11}\mathrm{C}$	22.	10	
	$\alpha + {}^{12}\mathrm{C}$	20.	3	10.82 (21%), 14.32 (17%)
	$\alpha + {}^{13}\mathrm{C}$	15.	14	

tabulated levels with parameters fixed from the fit [23,24], shown in the bottom panels of Figs. 4 and 5.

If the fit were perfect the two would coincide. As already discussed above, the distance between symbols and lines, for each reaction, can be interpreted as the systematic error associated to the analysis. This error can arise from the background present in the data but also from the global amount of excited particle unstable unknown levels in Figs. 4 and 5. Indeed some measured yields at the highest values of the relative energy do not correspond to tabulated levels and therefore they cannot be fitted by Eq. (4). However, it is clear that this uncertainty does not modify our observation about the opposite trend of measured cold isotopes and reconstructed "warm" isotopes.

4.1. Efficiency corrections

In order to calculate the efficiency of the employed apparatus for the measured correlation functions and extract the associated error on the extracted pre-fragments yields, we have followed the procedure of Refs. [32,33].

The efficiency function of the apparatus for the decay of "warm" fragments in the observed channels was determined by Monte Carlo calculations, taking into account the geometry of the

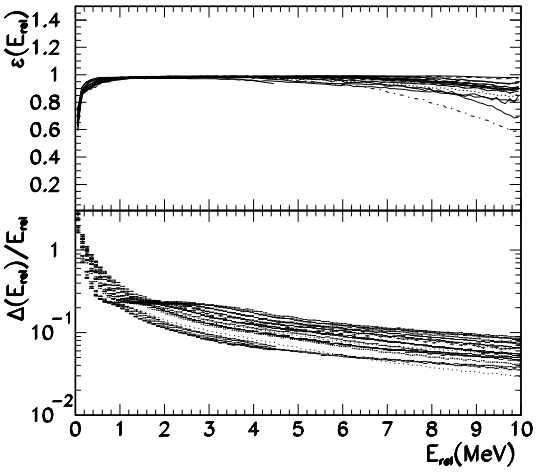

Fig. 9. (Color online.) Integral efficiency (top panel) and deviation (bottom panel) between the generated and detected relative energy as a function of the relative energy of detected particles for all the measured correlation functions.

detectors, the energy resolution, energy thresholds and the granularity of the telescopes. We assumed that the energy spectra and the angular distribution of excited parents have the same shape as those observed for stable fragments. For parent nuclei with particle unstable ground state, a distribution of neighboring stable nuclei was used to calculate the boost in the laboratory frame for the produced pair of daughters. The decay of parent nucleus was made isotropic in its rest frame. Only the angular range covered by the forward detector ($\theta = 5.3°$–$17.5°$), where detected particles and fragments are isotopically resolved, was considered for efficiency calculations.

The integral efficiency for each decay channel was defined [32] as the ratio between the yield of detected pairs and the number of generated pairs for each bin of relative energy. For a generated flat distribution of excitation energy of the parent nucleus (corresponding to a flat distribution of relative energy of the daughter particles) the integral efficiency shows a rapidly increasing trend in the first MeV of relative energy, starting from zero at zero relative energy, and reaching about 80% at 0.5 MeV. From about 1 MeV of relative energy on, the integral efficiency remains constant at about 90%, similarly to the case of other experimental devices with cylindrical arrangement of the detectors [35] around the beam axis. The reduced efficiency at small relative energies is due to the finite granularity and the rejection of double hits in the same telescope.

Since in the present experiment the identification of isotopes is obtained via the energy loss in the silicon detector, a double-hit of two particles in the same strip of the silicon detector cannot be recognized, resulting in a decrease of the parent yield. For instance, in the simulated decay of the ^{8}Be decaying in two α-particles, we found 2.5% of double hits in the same strip, corresponding to a relative energy smaller than 200 keV.

At high relative energies the efficiency results smaller when pairs of light particles or fragments are considered, as for instance p, d, ^{3,4}He and ^{6,7}Li, while the kinematics favors a higher efficiency in the case one of the two partners is heavier, as for instance Be, B or C.

To give some specific examples, the integral efficiency factors are found to be 79% and 95% for the $^{8}\mathrm{Be}_{\mathrm{g.s.}}$ and the 3.04 MeV excited state, respectively. In the case of the first excited state of ^{6}Li (2.186 MeV excitation energy) the integral efficiency resulted to be 88%.

The distortions on the widths of excited states, due to the finite opening angles of the individual telescopes, to the limited granularity of the experimental device and to low energy

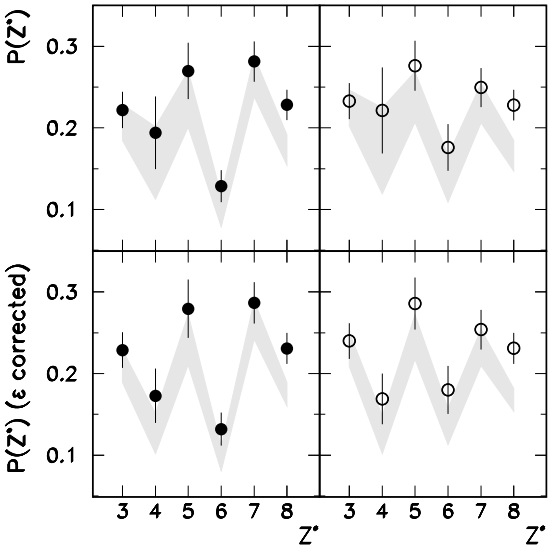

Fig. 10. (Color online.) Upper part: population of the different primary fragments (already shown in the panel a of Fig. 8). Lower part: population of the different primary fragments corrected for the integral efficiency of each correlation function. Data for peripheral events for $^{32}S + ^{58}Ni$ reaction are drawn as full symbols. Data for peripheral $^{32}S + ^{64}Ni$ reaction are drawn as circles. The grey regions represent the analog quantities for the fitting function Eq. (4).

cuts in the relative kinetic energy distribution was evaluated by comparing the generated and filtered relative energy spectra. We show in the bottom panel of Fig. 9 the deviation between the relative energy E_{rel} before the filter and the value E'_{rel} after the filtering procedure: $\Delta(E_{rel})/E_{rel} = |E_{rel} - E'_{rel}|/E_{rel}$. To this deviation very small contributions come from the finite energy resolution of the detector, typically less than 0.5% FWHM for the silicon strips [18].

We have also considered specific cases and we have evaluated the modifications of the FWHM of the relative energy distribution by the experimental device. To give some examples, for the 3.04 MeV excited state of ^{8}Be the detected FWHM is 2.3 MeV to be compared with the generated resonance width of 1.5 MeV. Much larger is the deformation of the $^{8}Be_{g.s.}$ emission, with a detected FWHM of 0.7 MeV instead of the generated 5.6 eV. In the case of the first excited state of ^{6}Li the FWHM after the filter is 0.447 MeV instead of the unfiltered 0.024 MeV, again similarly to other experimental devices [35]. Following this Monte Carlo simulation, the tabulated level widths in Eq. (4) smaller than 400 keV, were increased to account for the estimated efficiencies.

In Fig. 10 we show the fraction of the coincidence yield, corresponding to the emission by "warm" pre-fragments and defined in Eq. (5), before and after the integral efficiency correction [32] (top and bottom panels, respectively).

$$P_{corrected}(Z^*) = \frac{\sum_{A^*} \int Y(A^*, Z^*, E'_{rel}) \epsilon(E'_{rel}, E_{rel})^{-1} \, dE_{rel}}{\sum_{A^*} Y_{12}(A^*, Z^*)} \tag{6}$$

where E_{rel} is the actual relative energy, E'_{rel} is the measured one, and the integral efficiency $\epsilon(E'_{rel}, E_{rel})$ has been shown in Fig. 9.

Since the integral efficiency resulted quite high, as shown in Fig. 9, these corrections do not change the oscillating behavior observed in the left-bottom panel of Fig. 8.

4.2. Estimation of neutron decay

A limitation of our analysis is the systematic absence of neutron-decaying states in our reconstruction of excited levels, due to the lack of neutron detection. It is interesting that whenever an excited state has a known and finite probability of decaying through charged particle emission, the excited yield can be entirely reconstructed through Eq. (4) even if this channel is less important than neutron emission. However many excited states exist, especially in neutron rich isotopes, for which the charged particle branching ratio is negligible and that therefore are not included in our analysis.

One may then wonder if this systematic lack may be at the origin of the inverse staggering displayed in Figs. 8, 10.

To estimate the contribution of neutron decay we start writing the total yield of a given primary fragment (A^*, Z^*) as the sum of charged particle decay and neutral decay channels:

$$\begin{aligned} Y\big(A^*, Z^*\big) &= \sum_i Y\big(A^*, Z^*, i\big)(\text{B.R.})^i_{ch} + \sum_i Y\big(N^*, Z^*, i\big)(\text{B.R.})^i_n \\ &= Y_{ch}\big(A^*, Z^*\big) + Y_n\big(A^*, Z^*\big) \end{aligned} \tag{7}$$

where the sum runs over the particle unstable levels of the considered isotope, $(\text{B.R.})^i_{ch(n)}$ is the branching ratio of level i to charged (neutral) channels, and by definition $(\text{B.R.})^i_{ch} + (\text{B.R.})^i_n = 1$.

By writing the yield of each level $Y(A^*, Z^*, i)$ as a function of its spin, Boltzmann factor and branching ratios and by integrating the level contributions, one gets the total yield $Y_{n(ch)}(A^*, Z^*)$:

$$Y_{n(ch)}\big(A^*, Z^*\big) = g\big(A^*, Z^*\big) \sum_i (2J_i + 1) \exp\big(-E^*_i/T\big)(\text{B.R.})^i_{n(ch)} \tag{8}$$

where T is the average emission temperature, and the function g depends on the considered isotope (A^*, Z^*), on the characteristics of the emitting source (energy, mass, charge and angular momentum), but does not depend on the considered level i. Indeed the dependence on the level, i.e. on the good quantum numbers E^*_i, J_i, is already explicitly factorized in Eq. (8) under the hypothesis that the emission is governed by statistical laws.

If for a given isotope at least one energy level i exists such that $(\text{B.R.})^i_{ch} \neq 0$, then we can consider the ratio:

$$f\big(A^*, Z^*\big) = \frac{Y_n(A^*, Z^*)}{Y_{ch}(A^*, Z^*)} = \frac{\sum_{i=1}(2J_i + 1)\exp(-E^*_i/T)(\text{B.R.})^i_n}{\sum_i (2J_i + 1)\exp(-E^*_i/T)(\text{B.R.})^i_{ch}}. \tag{9}$$

This implies that we can build a correction factor for each isotope:

$$Y\big(A^*, Z^*\big) = Y_{ch}\big(A^*, Z^*\big)\big(1 + f\big(A^*, Z^*\big)\big) \tag{10}$$

where $Y_{ch}(A^*, Z^*) = Y_{cor(res)}(A^*, Z^*)$ represents the reconstructed, efficiency corrected yield obtained through correlation functions of charged decay products.

An example of this neutron correction is given by Fig. 11, which gives the mass distribution of reconstructed primary oxygen isotopes. For this correction we have considered in Eq. (9) all the tabulated particle unstable excited states up to the maximal excitation energy experimentally accessed in the charged channel decays. For the temperature parameter T we have taken $T = 2.5$ MeV, i.e. the average temperature measured by excited states thermometers for this same sample. This is consistent with the measured excitation energy of the peripheral sample,

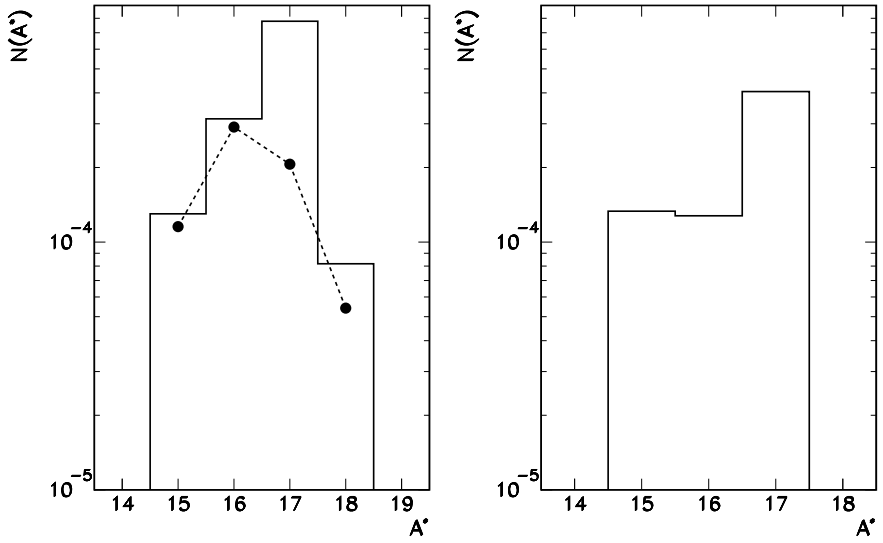

Fig. 11. (Color online.) Left part: Elemental mass distribution of primary oxygen fragments for $^{32}S + ^{58}Ni$ peripheral events, reconstructed with correlation functions with (solid histogram) and without (symbols connected by a dashed line) correction for neutron decay, Eq. (10). Right part: prediction of the GEMINI model at the last-but-one step of the decay.

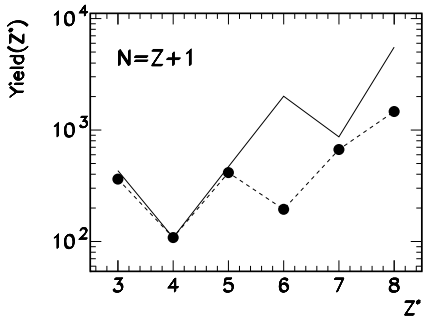

Fig. 12. (Color online.) Effect of neutron decay on the primary yields reconstructed with correlation functions for the isotopic chain $N = Z + 1$, for $^{32}S + ^{58}Ni$ peripheral events. Symbols connected by a line represent data not corrected for neutron decays. The continuous line corresponds to data corrected via Eq. (10).

assuming a level density parameter about $a = A/6$ [37,38]. As expected, the estimation of neutron contribution goes in the direction of increasing the yield of excited neutron-rich fragments, typically leading to an increase of one mass unit of the most probable isobar. The fact that the excited fragments result more neutron rich than the projectile may be somewhat surprising, but this is in qualitative agreement with GEMINI calculations, as shown in the right part of the same figure. The distribution of excited oxygen produced by the GEMINI calculation already optimized to describe this data set [16] shows indeed a yield of the neutron rich A = 17 isotope a factor 3 larger that lighter isotopes, even if the global width of the distribution appears overestimated. ^{17}O then decays in the last step in $n + ^{16}O$ with a 90% probability and in $\alpha + ^{13}C$ in the remaining cases.

Fig. 12 shows the global effect of this correction for neutron decay on the reconstructed primary yields for the $N = Z + 1$ isotopic chain. As it can be seen from Fig. 11 above, the effect

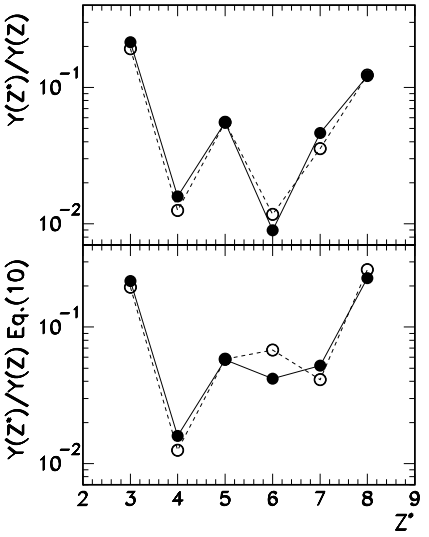

Fig. 13. (Color online.) Upper part: efficiency corrected population of the different primary fragments as extracted from correlation function. Lower part: estimation of the primary yields with a correction for neutron decay from Eq. (10). For both panels the reconstructed yield is normalized to the detected yield of the same element. Data for peripheral events for $^{32}S + ^{58}Ni$ reaction are drawn as full symbols. Data for peripheral $^{32}S + ^{64}Ni$ reaction are drawn as circles.

of this correction on $N = Z$ and $N = Z - 1$ is small, while the statistics for the isotopic chain $N = Z + 2$ is too low to make reliable estimations.

Odd–even effects persist in Fig. 12, showing that the absence of neutron detection cannot be at the origin of the observed staggering.

We show in Fig. 13 the yields of primary fragments, corrected for neutron decay contributions, normalized to the measured yield of the same element. Due to the impossibility of evaluating the non-coincident yield of neutral channels, we cannot indeed use the normalization of Eq. (5) and Figs. 8, 10.

We can see that the effect of neutron decay is more sizable in the more neutron rich source especially for oxygen isotopes, and slightly reduces the observed staggering. From a qualitative point of view, the same staggering observed for reconstructed primary fragments (Fig. 8) is present, again opposite to the trend of measured cold isotopes of Fig. 2.

GEMINI calculations again confirm our findings. Fig. 14 presents the same theoretical calculation as Fig. 3 above, where the solid line corresponds to an incomplete reconstruction of the last-but-one evaporation step obtained by ignoring neutrons decaying channels, as it is done in the experimental data. The similarity between the full and dashed curves in Fig. 14 confirms that the trend of the experimental "warm" distribution at the last-but-one evaporation step of Fig. 8 is not qualitatively distorted by the lack of neutron detection.

5. Conclusions

In this paper we have reported on an experimental study of staggering in $^{32}S + ^{58}Ni$ and $^{32}S + ^{64}Ni$ collisions at 14.5 A MeV, performed with the TANDEM–ALPI acceleration system at the Legnaro National Laboratory. The data collection was assured by the GARFIELD apparatus coupled to a high resolution annular detector for correlation measurements, the Ring Counter.

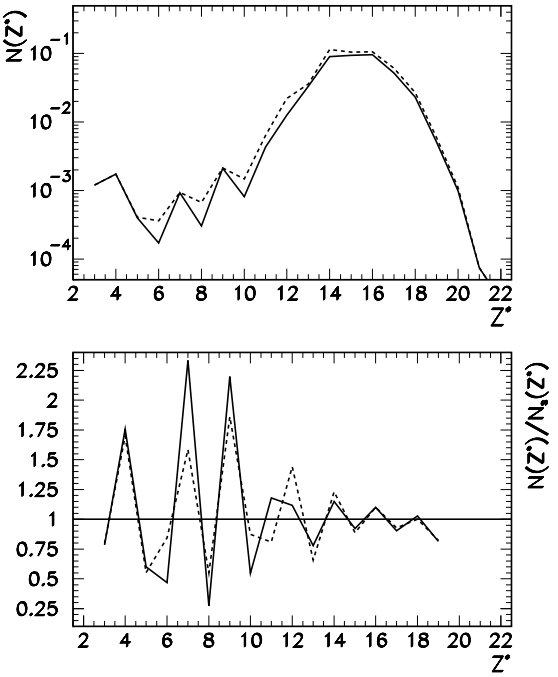

Fig. 14. (Color online.) Elemental "warm" fragment ($Z \geqslant 3$) distribution in the GEMINI model, with the same conditions as in Fig. 3 above. Solid lines: neutron decaying parents are not considered in the reconstruction of the excited yield.

Important odd–even effects are seen in the intermediate mass fragment yields as well as in the residue yields produced in the decay of a quasi-projectile sources formed in peripheral collisions.

For the light fragments ($3 \leqslant Z \leqslant 8$), which are the only ones isotopically resolved by the experimental apparatus, the discrete spectrum of excitation energy of "warm" pre-fragments extends over a wide energy range which can overcome the neutron and proton emission thresholds. This allows a partial reconstruction of the excited fragment yields prior to their last decay, through a model-independent correlation function technique.

This analysis shows that the distribution of excited fragments displays odd–even effects with an opposite sign in respect to the asymptotic distributions. This important result has a two-fold consequence. First, the quantitative understanding of the odd–even effect needs a global control of the evaporation chain. Second and more interesting, the understanding of the staggering cannot be attributed to the pairing effect of nuclear masses alone, but is also influenced by pairing and isospin effects in the level density. We expect it to be especially sensitive to the pairing effects in the level density via the back-shift parameter [39], and thus potentially useful to gather information of the temperature dependence of nuclear pairing.

First preliminary calculations with the GEMINI model confirm that staggering effects are present during the evaporation chain. The GEMINI distribution at the last-but-one evaporation step is in good qualitative agreement with the experimental correlation function data. This is however only a first step in the comparison, and further work is needed to fully constrain the level densities and different ingredients of the statistical calculations. Indeed it has been already observed [4,16] that important deviations appear when the behavior is analyzed in different isotopic chains. Limiting ourselves to the elemental distribution, an important discrepancy concerns

the relative yield of Li and Be isotopes, which is inverted in the calculation in respect to the trend shown by the experiment. Different explanations can be invoked to understand this discrepancy. First, the GEMINI code makes a switch from the Hauser–Feshbach formalism, used to describe light nuclei ($Z \leqslant 3$) evaporation, to the Bohr–Wheeler formalism, used to treat the emission of complex fragments heavier than Li. The absence of a unified description of fission and evaporation may be at the origin of the observed discrepancy. Moreover, the Be/Li ratio in the GEMINI code is sensitive to the value of the maximal angular momentum, which is poorly constrained in the experimental sample. Another problem concerns the treatment of the discrete particle unstable spectrum, which in GEMINI as in the other existing codes is approximated through a continuum level density. Our analysis shows that the discrete particle unstable states have to be explicitly included with their correct statistical weight, because they dominate the last evaporation step of light fragments.

From the experimental point of view, it is important to stress that the reconstruction of excited yields is only partial and some efforts should be made in the future to improve the situation.

The first is to improve the detector granularity so that more resonant states can be observed in the correlation functions. Our group is presently upgrading the set-up in this direction.

Moreover, a more abundant statistics is clearly needed for this exclusive analysis. In particular, since one would follow the evolution of the decay with increasing source excitation energy (i.e. the impact parameter), it is important to collect sufficient statistics to allow correlation functions analysis for bins of inelasticity.

In addition the analyses presented in this paper and those of Ref. [16] have to be performed for reactions where systematically the isospin of the emitting source is varied, by changing the combination of projectile and targets.

Finally, neutron detection would also be highly desirable to precisely trigger on the N/Z of the source and have a more quantitative control on isotopic effects on the last step of the de-excitation chain. However the branching ratios of the different decays for particle unstable levels of light fragments are typically experimentally known, or can be calculated through Hauser–Feshbach calculations. As we have explained, a sufficiently complete measurement of a given isotope through correlation functions can then allow to get also some quantitative information on the population of n-decaying levels. Alternatively this information can be deduced from the models if these latter are sufficiently constrained.

This will in the long run not only allow us to understand the origin of odd–even effects, but also to reconstruct primary fragments and thus access the thermodynamic information at the time of fragment formation, that is the temperature dependence of pairing and symmetry energy.

Acknowledgements

The authors are indebted to R. Cavaletti, L. Costa and A. Paolucci for the technical support during the experiment, M. Loriggiola for preparing the targets and M. Ottanelli for having realized the target-holder control system.

The authors also wish to thank the accelerator staff of the Tandem–Alpi complex of LNL (Laboratori Nazionali di Legnaro) for having provided high quality beams. The authors also wish to thank the LNL Program Advisory Committee, for the strong encouragement to complete our analyses.

One of the authors (Ad.R.R.) gratefully acknowledges the kind hospitality of INFN, Sezione di Bologna, where the work was partially done.

This work was supported in part by grants of Alma Mater Studiorum (Bologna University).

References

[1] L.B. Yang, et al., Phys. Rev. C 60 (1999) 041602, and references quoted therein.
[2] M.V. Ricciardi, et al., Nucl. Phys. A 733 (2004) 299, arXiv:1007.0386v1.
[3] G. Cardella, Limiting Collaboration, private communication;
I. Lombardo, et al., Int. J. Mod. Phys. E 20 (2011) 1066;
I. Lombardo, et al., Phys. Rev. C 84 (2011) 024613.
[4] E. Bonnet, J.P. Wieleczko, et al., Int. J. Mod. Phys. E 17 (2009) 2359;
G. Ademard, et al., Phys. Rev. C 83 (2011) 054619.
[5] E. Geraci, et al., Nucl. Phys. A 732 (2004) 173.
[6] A. Schiller, et al., Phys. Rev. C 63 (2001) 021306(R).
[7] N. Chamel, et al., Phys. Rev. C 81 (2010) 045804.
[8] A. Fantina, et al., Phys. Lett. B 676 (2009) 140.
[9] M. Colonna, F. Matera, Phys. Rev. C 71 (2005) 064605.
[10] S. Wuenschel, et al., Phys. Rev. C 79 (2009) 061602(R).
[11] Ad.R. Raduta, F. Gulminelli, Phys. Rev. C 75 (2007) 044605.
[12] R.J. Charity, et al., Phys. Rev. C 63 (2001) 024611.
[13] C. Dorso, et al., arXiv:1105.0050v1.
[14] A. Ono, AIP Conf. Proc. 884 (2007) 292.
[15] J. Su, F. Zhang, B. Bian, Phys. Rev. C 83 (2011) 014608.
[16] M. D'Agostino, et al., Nucl. Phys. A 861 (2011) 47.
[17] F. Gramegna, et al., Nucl. Instr. Meth. A 389 (1997) 474;
IEEE Nucl. Science Symposium, Rome, 16–22 October 2004.
[18] A. Moroni, et al., Nucl. Instr. Meth. A 556 (2006) 516.
[19] J. Cugnon, D. L'Ĥote, Nucl. Phys. A 397 (1983) 519.
[20] N. Marie, et al., Phys. Lett. B 391 (1997) 15.
[21] M. D'Agostino, et al., Phys. Lett. B 368 (1996) 259.
[22] R.J. Charity, Phys. Rev. C 82 (2010) 014610.
[23] F. Gulminelli, D. Durand, Nucl. Phys. A 615 (1997) 117.
[24] http://www.nndc.bnl.gov/nudat2/.
[25] R. Hanbury Brown, R.Q. Twiss, Philos. Mag. 45 (1954) 663;
R. Hanbury Brown, R.Q. Twiss, Nature (London) 177 (1956) 27;
R. Hanbury Brown, R.Q. Twiss, Nature (London) 178 (1956) 1046.
[26] D.H. Boal, C.K. Gelbke, B.K. Jennings, Rev. Mod. Phys. 62 (1990) 553.
[27] M.A. Lisa, et al., Ann. Rev. Nucl. Part. Sci. 55 (2005) 337.
[28] V. Henzl, et al., arXiv:1108.2552v1, and references therein.
[29] J. Lecouey, et al., Phys. Lett. B 672 (2009) 6.
[30] R. Trockel, et al., Phys. Rev. Lett. 59 (1987) 2844.
[31] O. Shapiro, D.H.E. Gross, Nucl. Phys. A 573 (1994) 143.
[32] J. Pochodzalla, et al., Phys. Rev. C 35 (1987) 1695.
[33] T.K. Nayak, et al., Phys. Rev. C 45 (1992) 132.
[34] W.P. Tan, et al., Phys. Rev. C 69 (2004) 061304(R).
[35] M. Assenard, INDRA Collaboration, SUBATECH 97-15, LPPC97-11.
[36] J.P. Bondorf, A.S. Botvina, A.S. Iljinov, I.N. Mishustin, K. Sneppen, Phys. Rep. 257 (1995) 133.
[37] J. Toke, W.J. Swiatecki, Nucl. Phys. A 372 (1981) 141.
[38] A.V. Voinov, et al., Phys. Rev. C 76 (2007) 044602.
[39] Y. Alhassid, G.F. Bertsch, L. Fang, Phys. Rev. C 68 (2003) 044322.